Optics Letters

Gas spectroscopy with integrated frequency monitoring through self-mixing in a terahertz quantum-cascade laser

Rabi Chhantyal-Pun, Alexander Valavanis,* James T. Keeley, Pierluigi Rubino, Iman Kundu, Yingjun Han, Paul Dean, Lianhe Li, A. Giles Davies, and Edmund H. Linfield

Institute of Microwaves and Photonics, School of Electronic and Electrical Engineering, University of Leeds, Leeds LS2 9JT, UK
**Corresponding author: a.valavanis@leeds.ac.uk*

Received 15 February 2018; accepted 12 March 2018; posted 15 March 2018 (Doc. ID 323151); published 2 May 2018

We demonstrate a gas spectroscopy technique, using self-mixing in a 3.4 terahertz quantum-cascade laser (QCL). All previous QCL spectroscopy techniques have required additional terahertz instrumentation (detectors, mixers, or spectrometers) for system pre-calibration or spectral analysis. By contrast, our system self-calibrates the laser frequency (i.e., with no external instrumentation) to a precision of 630 MHz (0.02%) by analyzing QCL voltage perturbations in response to optical feedback within a 0–800 mm round-trip delay line. We demonstrate methanol spectroscopy by introducing a gas cell into the feedback path and show that a limiting absorption coefficient of $\sim 1 \times 10^{-4}$ cm^{-1} is resolvable.

OCIS codes: (140.5965) Semiconductor lasers, quantum cascade; (300.6495) Spectroscopy, terahertz; (120.3180) Interferometry.

https://doi.org/10.1364/OL.43.002225

Terahertz-frequency quantum-cascade lasers (THz QCLs) [1] are attractive radiation sources for terahertz gas spectroscopy, compared with photomixers or gas lasers, owing to their compact size, high emission powers (>2.4 W pulsed [2], >100 mW continuous-wave [cw] [3]), narrow instantaneous free-running linewidth (<30 kHz [4]), and their availability across the 1.2–5.4 THz range [5,6]. Several THz-QCL gas spectroscopy techniques have been demonstrated, including direct-transmission [7], frequency modulation [8], heterodyne radiometry [9], and photoacoustic techniques [10]. Recently, a self-mixing (SM) interferometry method has also been developed [11,12]. In SM techniques [13], terahertz radiation is intentionally reflected back into the QCL, causing interference within the laser. This induces changes in the QCL terminal voltage, which are sensitive to both the amplitude and phase of the reflected field, and this has underpinned a wide range of terahertz applications, including imaging [14,15] and materials analysis [16].

To date, however, all THz-QCL spectroscopy approaches have required external terahertz instrumentation (detectors, mixers, or spectrometers), in addition to the QCL for power monitoring or pre-calibration of the laser frequency, potentially increasing the system cost and reliance on specialist components. Pre-calibrated systems also lack robustness against long-term laser-frequency drifts, for example, through thermal-environmental changes. In this Letter, we extend the SM spectroscopy concept by introducing an adjustable optical delay into the feedback path, enabling the acquisition of long-path interferograms. Through this approach, we infer the laser frequency-tuning characteristics directly, without external calibration.

The QCL used in this Letter is based on the active-region (AR) design described in Ref. [17], which was dimensionally rescaled to a ~3.4–3.6 THz gain bandwidth. The structure was grown on a semi-insulating GaAs substrate using molecular beam epitaxy. An initial 250 nm thick GaAs buffer was followed by a 300 nm thick $Al_{0.5}Ga_{0.5}As$ etch-stop layer and a 700 nm thick *n*-GaAs contact layer, which was Si-doped to a density of $\rho = 2 \times 10^{18}$ cm^{-3}. 117 periods of the AR were then grown to a thickness of ~14.5 μm, followed by a second 50 nm thick *n*-GaAs ($\rho = 5 \times 10^{18}$ cm^{-3}) top-contact layer. A 150 μm wide Au-plasmonic ridge-waveguide structure was defined lithographically and cleaved to a length of 1.8 mm. Single-mode emission was achieved by focused-ion-beam milling a 160 μm long photonic lattice through the top contact layers, using a 12.8 μm grating period with a 60% duty cycle and a central 9 μm wide phase defect as in [18]. The QCL was operated in cw mode at 20 K heat-sink temperature within a Janis ST-100 helium cryostat, using an Arroyo 4302 current source. A maximum cw operating temperature of ~60 K, a threshold current of 450 mA, and a peak optical power output of ~12 mW (at ≤ 20 K) were measured.

The optical and electronic configuration of our gas spectroscopy system is illustrated schematically in Fig. 1. Terahertz radiation from the QCL was collimated using an Al-plated 25 mm diameter, 75 mm effective focal length 90° off-axis paraboloidal mirror, and directed through a 96.5 cm long glass gas cell, with 4 mm thick polymethylpentene Brewster-angle windows, which provide low-loss flat-band terahertz transmission. A planar

elliptical cross-sectional Au-plated mirror was used to direct the transmitted beam onto a pair of identical mirrors in a beam-folding arrangement, which were mounted onto a 200 mm long Newport ILS-200 mechanical translation stage. The optical system was completed with a final circular cross-sectional planar mirror, which was used to reflect the terahertz beam along the same optical path and back into the QCL cavity.

A Newport XPS-Q8 motion controller was used to translate the beam-folding mirrors longitudinally along the beam path, allowing a variable 0–800 mm (0–2.66-ns) round-trip delay to be introduced into the optical path. The motion control system was configured to generate electronic trigger-output pulses at 2 μm intervals along the motion path. The voltage across the QCL terminals was monitored using an ac-coupled National Instruments data acquisition (NI-DAQ) board, such that only the time-varying SM-induced perturbations were recorded. The position-trigger pulses were used as an external clock input, hence allowing the SM signal to be tabulated accurately as a function of the optical delay within the system.

Using the measurement approach described above, a constant dc current was used to bias the QCL, and the delay stage was translated over its full length at a speed of 100 mms^{-1}. The resulting phase shift in the terahertz feedback led to a periodic SM interference effect being generated in the QCL, and the corresponding voltage perturbations $v_{\text{SM}}(t)$ were recorded as a function of the round-trip delay time. A fast Fourier transform (FFT) was used to obtain the frequency spectrum of the interferogram, and a regression to a Gaussian function was used to determine the principal frequency component of the signal (i.e., the QCL emission frequency). In these measurements, the maximum 800 mm round-trip delay corresponds to an FFT sampling resolution of around 380 MHz, and the 2 μm step size corresponds to an FFT spectral bandwidth of 37 THz. As such, the analysis is unaffected by aliasing, and provides a comparable spectral resolution to commercial Fourier transform infrared (FTIR) spectrometers. In addition to obtaining the QCL emission frequency, the amplitude of the Gaussian fit provides a measure of the transmitted intensity.

Figure 2 shows an exemplar SM spectrum obtained using this method, with the QCL biased to obtain its peak output power ($I = 549.8$ mA) and the gas cell under vacuum. The dataset [19] contains all research data associated with this Letter. The QCL generates a single-mode emission profile under these biasing conditions at a frequency of 3.4048 THz, and the Gaussian function provides a good fit (adjusted $R^2 > 0.95$) to the FFT.

These measurements were repeated at different QCL drive current values to obtain an initial estimate of the tuning characteristics across the full 500–600 mA single-mode operation range of the QCL at 1 mA increments. To improve data acquisition speed, data were recorded with the translation stage moving in forward or reverse directions for adjacent current values. As such, a data acquisition rate of 0.5 samples/s was obtained, giving a total scan time of 50 s for Fig. 3. As a post-processing step, the FFT output parameters (i.e., frequency and amplitude) from adjacent forward and reverse scans were averaged to remove SM hysteresis effects. The inferred QCL frequency, f, is shown in Fig. 3, to vary with respect to current, I, across the 3.4045–3.4051 THz range. The usable frequency resolution of this data (in common with all FFT techniques) is limited by the length of the interferogram. As such, plateaus are clearly visible in the plot, separated by the 380 MHz FFT bin resolution. The apparent "smoothing" of these features is a result of the Gaussian fitting process, which introduces a degree of interpolation or oversampling between the FFT frequency bins. The measurement was repeated with the gas cell filled with 1100 mTorr (150 Pa) of methanol vapor (black line in Fig. 3). Although the SM effect causes small perturbations in the emission frequency, this was found to be significantly smaller than the FFT frequency bin size and, as such, their true magnitude cannot be stated with accuracy. A curve-fitting approach was used to estimate the true underlying QCL tuning characteristics from the experimental FFT data. Therefore, linear fittings to the two measurements (with and without methanol present) of the form $f = f_0 + \beta I$ were averaged to obtain an approximate *in situ* frequency–current calibration for our subsequent measurements (blue line in Fig. 3). The resulting parameters were found to be $f_0 = 3.4012$ THz and $\beta = 6.472\ \text{MHz mA}^{-1}$. Some nonlinearity of the true QCL tuning function can be expected, particularly when subject to feedback. However, since the FFT data cover less than three frequency bins, higher-order polynomial fittings cannot be extracted with any accuracy. This situation could potentially be improved through the use of a more widely tunable QCL or a longer translation stage.

The QCL SM voltage modulation amplitude can be described as a function of the round-trip phase delay [11], using

$$v_{\text{SM}}(\phi_0) \propto T\cos[\phi_0 - C\sin(\phi - \arctan(\alpha))], \quad \textbf{(1)}$$

where $\phi_0 = 2\pi\nu_0\tau$ is the round-trip phase delay as a function of the QCL frequency ν_0 and the external cavity round-trip

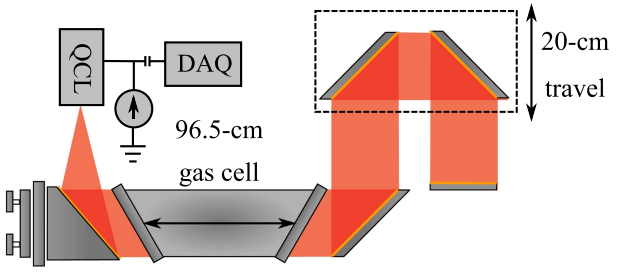

Fig. 1. Schematic illustration of the configuration of the gas spectroscopy system. An ac-coupled National Instruments data acquisition board was used to record the SM-induced perturbations to the QCL terminal voltage.

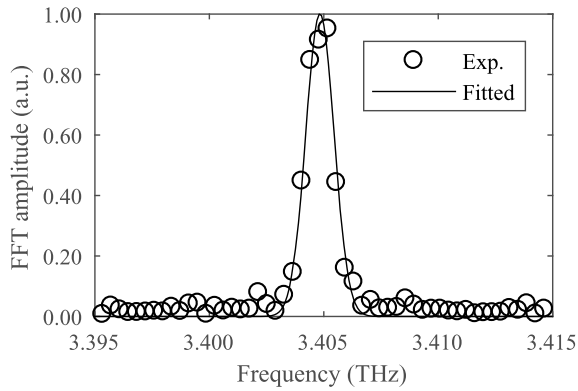

Fig. 2. FFT spectrum obtained from a SM interferogram at a 549.8 mA dc drive current and with the gas cell under vacuum. The solid line shows a Gaussian fit to the experimental data (circles).

time τ. The SM effect, in general, leads to a small shift in the round-trip phase delay, and strictly the perturbed value ϕ in the equation above will be slightly different from ϕ_0. The terms C and α denote the feedback strength and the linewidth enhancement factor of the QCL, respectively. The most significant parameter for gas spectroscopy is the single-pass Beer–Lambert power transmission factor $T = \exp(-\alpha_{\text{gas}} L_{\text{gas}})$ which, in turn, depends on the absorption coefficient α_{gas} of the gas and the length of the gas cell L_{gas}.

Equation (1) can be simplified to a closed analytical form, by assuming that $C \ll 1$ (i.e., weak feedback), such that $v_{\text{SM}}(\tau) \propto \exp(-\alpha_{\text{gas}} L_{\text{gas}}) \cos(2\pi\nu_0\tau)$. This approximation is intuitively justified by the long external feedback path and by the relatively small SM frequency-pulling effects in Fig. 3. The amplitude of the SM interferogram A, therefore, is expected to be proportional to the terahertz power transmission factor. As such, the gas absorption coefficient may be obtained using the familiar Beer–Lambert law: $\alpha_{\text{gas}}(I) = L_{\text{gas}}^{-1} \ln[A_0(I)/A(I)]$, where A and A_0 are the respective SM signal amplitudes measured with and without the gas present within the cell.

To demonstrate the validity of this approach, the gas cell was filled with 1100 mTorr methanol vapor, and α_{gas} was determined at each QCL bias current in the range shown in Fig. 3. The QCL frequency at each step was estimated using the *in situ* calibration described above. The resulting absorption spectrum is plotted in Fig. 4 and shows that two distinct methanol absorption peaks are resolved. A fine calibration of the absolute frequency scale was obtained by referencing these peaks to a simulated spectrum, using cataloged data from [20]. The cataloged integrated absorption coefficient values were convolved with a Voigt profile to account for self-broadening at 1100 mTorr, giving a full-width at half-maximum (FWHM) of 30 MHz and a Doppler broadening (FWHM 10 MHz) at room temperature. The self-broadening value was obtained from the HITRAN database [21] and is the dominant line-broadening mechanism. The simulated spectrum was found to contain a pair of lines at 3.40402 and 3.40436 THz, with the same relative spacing as the experimental SM data, and absorption coefficients of $\sim 1 \times 10^{-2}$ cm^{-1} in each case. The *in situ* frequency–current calibration described above, therefore, was corrected by an absolute −0.63 GHz (−0.02%) shift. This corresponds to 1.7× the FFT resolution and may be attributed to a small calibration offset in the motion control system. Such effects could feasibly be negated through the inclusion of a He:Ne reference laser mounted collinearly with the terahertz beam, as commonly found in commercial FTIR systems.

For comparison, Fig. 4 also shows spectra obtained using a conventional direct transmission measurement through the gas cell. This was obtained by placing a mechanical chopper into the terahertz beam path, at a modulation frequency of 167 Hz, and measuring the terahertz power transmitted through the gas cell using a pyroelectric detector. The time-averaged detector output was recorded using a lock-in amplifier, which was referenced to the chopper frequency. The frequency scale for the direct measurement was obtained using the same frequency–current mapping as that determined for the SM measurements. The absorption spectrum obtained from the SM method gives a similar peak absorption coefficient, compared to the direct method, for the same methanol pressure.

To assess the sensitivity and linearity of the SM analysis scheme, the pressure of the methanol vapor was varied, and the measurement was repeated. Figure 5 shows that the peak intensity increases linearly with respect to the vapor pressure, as expected from the Beer–Lambert law. However, the linewidth of the transition appears to decrease slightly with increasing methanol pressure, in contrast to the normal pressure dependence of gas transitions. This anomaly is principally a result of the weak feedback approximation used in the data analysis (i.e., the assumption that SM effects do not perturb the laser frequency). Indeed, Fig. 3 shows that small SM-induced frequency perturbations do occur at currents corresponding to the two absorption lines, with the magnitude of the perturbation depending on the feedback strength. This effect could potentially be mitigated through the use of higher-resolution time-domain measurements of the SM signal to extract the feedback parameter, C, and estimate the magnitude of the frequency pulling.

A minimum detectable absorption coefficient of $\sim 1.0 \times 10^{-4}$ cm^{-1}, corresponding to ∼10 mTorr of methanol or 3×10^{14} molecule/cm^3, was inferred by extrapolating the data in Fig. 5(b) back to the standard deviation of the baseline absorbance. This was obtained from repeated measurements of the SM amplitude at a fixed current corresponding to 3.40436 THz absorption feature.

In conclusion, we have demonstrated an SM interferometry technique for terahertz-frequency gas spectroscopy, in which an

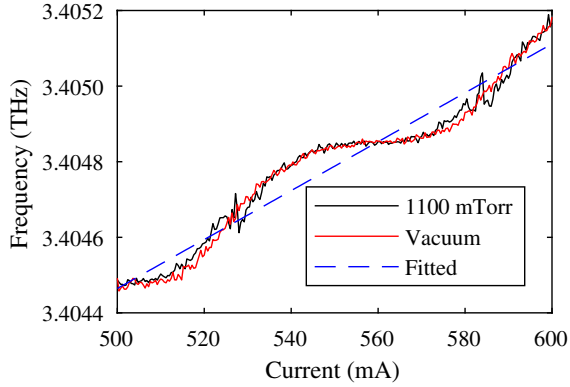

Fig. 3. Inferred QCL emission frequency as a function of the driving current with the sample cell under vacuum and filled with 1100 mTorr methanol vapor. The dashed line shows a linear fitting to the experimental measurements.

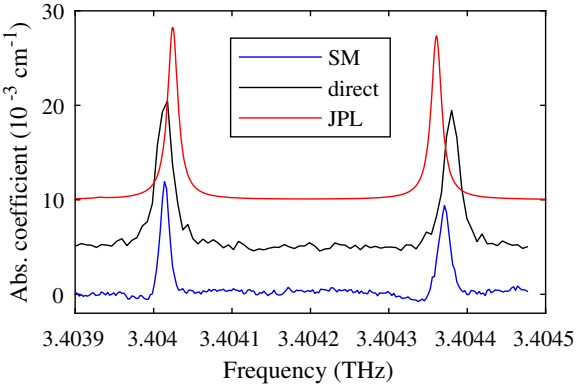

Fig. 4. Methanol spectra obtained using various methods. The blue and black traces show experimental SM and direct transmission measurements, respectively. The red trace shows a simulation using data from Ref. [20], against which the QCL frequency has been finely calibrated.

optical delay stage is used for *in situ* calibration of the QCL frequency-tuning characteristics to within an absolute accuracy of 0.02%. This method provides a key advantage over previous QCL-based approaches in that this is the first such method that removes the need for any specialized terahertz instrumentation external to the QCL itself. Whereas previous techniques have required *a priori* calibration using costly external apparatus (e.g., FTIR spectrometers) or molecular reference cells, our technique directly infers the QCL frequency from SM interferometric measurements. Since the calibration capability is intrinsic to the system, our technique is inherently resilient against drifts in the laser characteristics (e.g., through changes in temperature or power supply drift) and, therefore, potentially better suited to long-term deployment in industrial applications or in atmospheric-sensing field measurements. We have shown that the system provides a linear pressure dependence, as expected from the Beer–Lambert law, and have estimated a sensitivity limit of ~0.0001 cm^{-1} absorption coefficient. The capabilities of this technique could be enhanced relatively simply through the incorporation of a longer and higher-precision optical delay path to improve frequency resolution and a more widely tunable QCL to improve the spectral bandwidth. The feasibility of use in industrial or field applications could also be enhanced through the use of a compact closed-cycle cooler system in preference to a helium cryostat. Longer-term enhancements could be realized through the use of cavity-enhanced sensing or multi-pass gas cell arrangements.

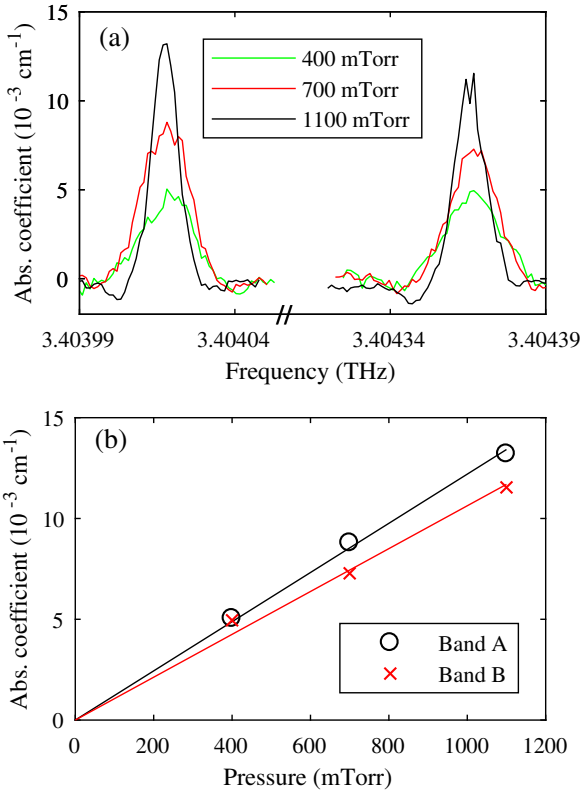

Fig. 5. (a) Methanol spectra as a function of vapor pressure, using a frequency scale calibrated against cataloged spectral lines [20]. (b) Peak intensities as a function of vapor pressure. Solid lines show linear fits to the data points. Bands A and B refer to the lower and higher frequency spectral lines, respectively.

Funding. Royal Society (WM150029); Engineering and Physical Sciences Research Council (EPSRC) (EP/J017671/1, EP/P021859/1).

Acknowledgment. The authors thank A. Orr-Ewing, University of Bristol, UK, for the provision of a gas cell, and J.-C. Gómez Martín and J. Plane, University of Leeds, UK, for assistance in the development of a methanol vapor delivery manifold system.

REFERENCES

1. R. Köhler, A. Tredicucci, F. Beltram, H. E. Beere, E. H. Linfield, A. G. Davies, D. A. Ritchie, R. C. Iotti, and F. Rossi, Nature **417**, 156 (2002).
2. L. H. Li, L. Chen, J. R. Freeman, M. Salih, P. Dean, A. G. Davies, and E. H. Linfield, Electron. Lett. **53**, 799 (2017).
3. B. Williams, S. Kumar, Q. Hu, and J. Reno, Electron. Lett. **42**, 89 (2006).
4. A. Barkan, F. K. Tittel, D. M. Mittleman, R. Dengler, P. H. Siegel, G. Scalari, L. Ajili, J. Faist, H. E. Beere, E. H. Linfield, A. G. Davies, and D. A. Ritchie, Opt. Lett. **29**, 575 (2004).
5. C. Walther, M. Fischer, G. Scalari, R. Terazzi, N. Hoyler, and J. Faist, Appl. Phys. Lett. **91**, 131122 (2007).
6. M. Wienold, B. Röben, X. Lü, G. Rozas, L. Schrottke, K. Biermann, and H. T. Grahn, Appl. Phys. Lett. **107**, 202101 (2015).
7. H.-W. Hübers, S. G. Pavlov, H. Richter, A. D. Semenov, L. Mahler, A. Tredicucci, H. E. Beere, and D. A. Ritchie, Appl. Phys. Lett. **89**, 061115 (2006).
8. R. Eichholz, H. Richter, M. Wienold, L. Schrottke, R. Hey, H. T. Grahn, and H.-W. Hübers, Opt. Express **21**, 32199 (2013).
9. H. Richter, A. D. Semenov, S. G. Pavlov, L. Mahler, A. Tredicucci, H. E. Beere, D. A. Ritchie, K. S. Il'in, M. Siegel, and H.-W. Hübers, Appl. Phys. Lett. **93**, 141108 (2008).
10. P. Patimisco, S. Borri, A. Sampaolo, H. E. Beere, D. A. Ritchie, M. S. Vitiello, G. Scamarcio, and V. Spagnolo, Analyst **139**, 2079 (2014).
11. T. Hagelschuer, M. Wienold, H. Richter, L. Schrottke, K. Biermann, H. T. Grahn, and H.-W. Hübers, Appl. Phys. Lett. **109**, 191101 (2016).
12. T. Hagelschuer, M. Wienold, H. Richter, L. Schrottke, H. T. Grahn, and H.-W. Hübers, Opt. Express **25**, 30203 (2017).
13. Y. L. Lim, P. Dean, M. Nikolić, R. Kliese, S. P. Khanna, M. Lachab, A. Valavanis, D. Indjin, Z. Ikonić, P. Harrison, E. H. Linfield, A. G. Davies, S. J. Wilson, and A. D. Rakić, Appl. Phys. Lett. **99**, 081108 (2011).
14. P. Dean, Y. L. Lim, A. Valavanis, R. Kliese, M. Nikolić, S. P. Khanna, M. Lachab, D. Indjin, Z. Ikonić, P. Harrison, A. D. Rakić, E. H. Linfield, and A. G. Davies, Opt. Lett. **36**, 2587 (2011).
15. J. Keeley, P. Dean, A. Valavanis, K. Bertling, Y. L. Lim, R. Alhathlool, T. Taimre, L. H. Li, D. Indjin, A. D. Rakić, E. H. Linfield, and A. G. Davies, Opt. Lett. **40**, 994 (2015).
16. S. Han, K. Bertling, P. Dean, J. Keeley, A. D. Burnett, Y. L. Lim, S. P. Khanna, A. Valavanis, E. H. Linfield, A. G. Davies, D. Indjin, T. Taimre, and A. D. Rakić, Sensors **16**, 352 (2016).
17. M. Wienold, L. Schrottke, M. Giehler, R. Hey, W. Anders, and H. Grahn, Electron. Lett. **45**, 1030 (2009).
18. I. Kundu, P. Dean, A. Valavanis, L. Li, Y. Han, E. H. Linfield, and A. G. Davies, IEEE Trans. Terahertz Sci. Technol. **7**, 360 (2017).
19. R. Chhantyal-Pun, A. Valavanis, J. T. Keeley, P. Rubino, I. Kundu, Y. Han, P. Dean, L. Li, A. G. Davies, and E. H. Linfield, https://doi.org/10.5518/204 (University of Leeds, 2017).
20. H. M. Pickett, R. L. Poynter, E. A. Cohen, M. L. Delitsky, J. C. Pearson, and H. S. P. Müller, J. Quant. Spectrosc. Radiat. Transfer **60**, 883 (1998).
21. L. S. Rothman, I. E. Gordon, Y. Babikov, A. Barbe, D. Chris Benner, P. F. Bernath, M. Birk, L. Bizzocchi, V. Boudon, L. R. Brown, A. Campargue, K. Chance, E. A. Cohen, L. H. Coudert, V. M. Devi, B. J. Drouin, A. Fayt, J. M. Flaud, R. R. Gamache, J. J. Harrison, J. M. Hartmann, C. Hill, J. T. Hodges, D. Jacquemart, A. Jolly, J. Lamouroux, R. J. Le Roy, G. Li, D. A. Long, O. M. Lyulin, C. J. Mackie, S. T. Massie, S. Mikhailenko, H. S. P. Müller, O. V. Naumenko, A. V. Nikitin, J. Orphal, V. Perevalov, A. Perrin, E. R. Polovtseva, C. Richard, M. A. H. Smith, E. Starikova, K. Sung, S. Tashkun, J. Tennyson, G. C. Toon, V. G. Tyuterev, and G. Wagner, J. Quant. Spectrosc. Radiat. Transfer **130**, 4 (2013).